Multiple Higher-Order Stop Gaps in Infrared Polymer Photonic Crystals

M. Straub, M. Ventura, and M. Gu

*Centre for Micro-Photonics and ARC Centre of Excellence for Ultrahigh-Bandwidth Devices for Optical Systems,
School of Biophysical Sciences and Electrical Engineering, Swinburne University of Technology,
PO Box 218, Hawthorn, Victoria 3122, Australia*

Engineering of stop gaps between higher photonic bands provides an alternative to miniaturization of photonic crystals. Femtosecond laser microfabrication of highly correlated void channel polymer microstructures results in photonic crystals with large stop gaps and a multitude of higher-order gaps in the mid- and near-infrared spectral regions. The gap wavelengths obey Bragg's law. Consistent with theory, varying the woodpile structure unit cell allows for tuning the number of higher-order gaps, and transitions from mere resonant Bragg scattering to stop band total reflection are observed.

Despite their potential to manipulate light propagation in the technological relevant near-infrared and visible wavelength regions at much larger structural dimensions, there has been relatively little experimental work to date on photonic crystals with higher-order stop bands [1–11]. As higher-order stop gaps correspond to higher-order Bragg scattering, they are a general feature of photonic crystals, whereas complete higher-order band gaps have been predicted only in exceptional cases [12–14]. Subsequent to first experiments on mechanically machined silicon woodpile structures by terahertz spectroscopy [1], various approaches led to the observation of higher-order stop gaps. For face-centered cubic structures of submicron air spheres in titania in the frequency range of the (222)-Bragg diffraction three higher-order stop gaps were observed [2], the one between the eighth and ninth band almost being a complete photonic band gap [14]. Similar gaps prevail in inverse opals generated by electrodeposition of II-VI semiconductor materials [3] and chemical vapor deposition of silicon [4,5], the latter even featuring a complete band gap. Higher-order stop gaps were also observed in triangular patterns of photoelectrochemically etched cylindrical holes in bulk silicon, which were used as a microreflectors [6]. Recently, photonic crystals generated by two-photon photopolymerization allowed for the observation of higher-order stop gaps at near-infrared wavelengths [7]. Other investigations on self-assembled particles comprise multiple Bragg reflections recorded by visible and ultraviolet spectrophotometry [8] or small-angle x-ray diffraction [9], as well as UV-vis transmission spectra [10,11], but do not give direct evidence of a stop gap or distinguish from mere secondary diffraction by differently oriented lattice planes [15].

Photonic crystals with higher-order stop gaps are not easily fabricated, as they require highly correlated structural arrangements with a minimum of defects. Recently, we have developed a method to generate infrared photonic crystals by femtosecond laser drilling in solid polymer blocks [16]. Arranging only 20 layers of void

channels with submicron diameter in a woodpile structure allowed for the suppression of infrared transmission in the stacking direction by as much as 85%. The high degree of channel perfection and the large variety of achievable lattice types and unit cell geometries qualify this technique uniquely for the observation of higher-order stop gaps in the near-infrared spectral region. Intrinsic defects or polymer shrinkage does not play a significant role. The fabrication is a one-step approach, which is carried out within a few tens of minutes using commercially available material and does no require additional chemical processing, unless complete band gaps are desired.

In this Letter, we demonstrate that void channel polymer photonic crystals not only feature large fundamental stop gaps in the 4–8 μm wavelength range, but also provide a multitude of sizable higher-order gaps. The number of higher-order stop gaps can be selected by changing the ratio between the layer spacing and the in-plane channel spacing of a woodpile structure. Gap/midgap ratios can be tuned by changing the filling ratio of the structures. The emergence of higher-order gaps manifests itself by the appearance of pronounced dips in the infrared transmission and a sharp increase in the intensity of Bragg reflections. Structural parameters of the crystals are determined by comparing their infrared spectra with photonic band structure calculations.

Void channels were generated by focusing femtosecond pulsed visible light from a Ti:sapphire laser combined with an optical parametric oscillator with an intracavity frequency doubler ($\lambda = 540$ nm, average power 14 mW, repetition rate 76 MHz, pulse width 200 fs) into a solid UV-cured Norland NOA63 optical adhesive via a Zeiss numerical aperture (NA) 1.3 objective [16]. Stage scanning of straight lines at scan speeds of 300 μm/s led to an elliptical channel cross section with a lateral diameter of approximately 750 nm and an elongation of approximately 50% in the focusing direction. Photonic crystals consisted of 20 layers of channels stacked in 80×80 μm

woodpile structures. Layer spacings δz varied from 1.6 to 2.7 μm with in-plane channel spacings δx ranging from 1.1 to 2.6 μm. Photonic stop gaps were measured using a Nicolet Nexus Fourier transform infrared spectrometer combined with a Continuum infrared microscope [32× NA 0.65 objective and condensor, 200 (1600) scans in transmission (reflection) at 4 cm^{-1} resolution].

Photonic band structures were calculated using an iterative eigensolver program [17]. Figure 1(a) shows two examples with a layer spacing of $\delta z = 2.5$ μm, but different ratios of the layer spacing to the in-plane channel spacing $\delta z/\delta x = 1.0$ (right) and 2.0 (left, only stack-
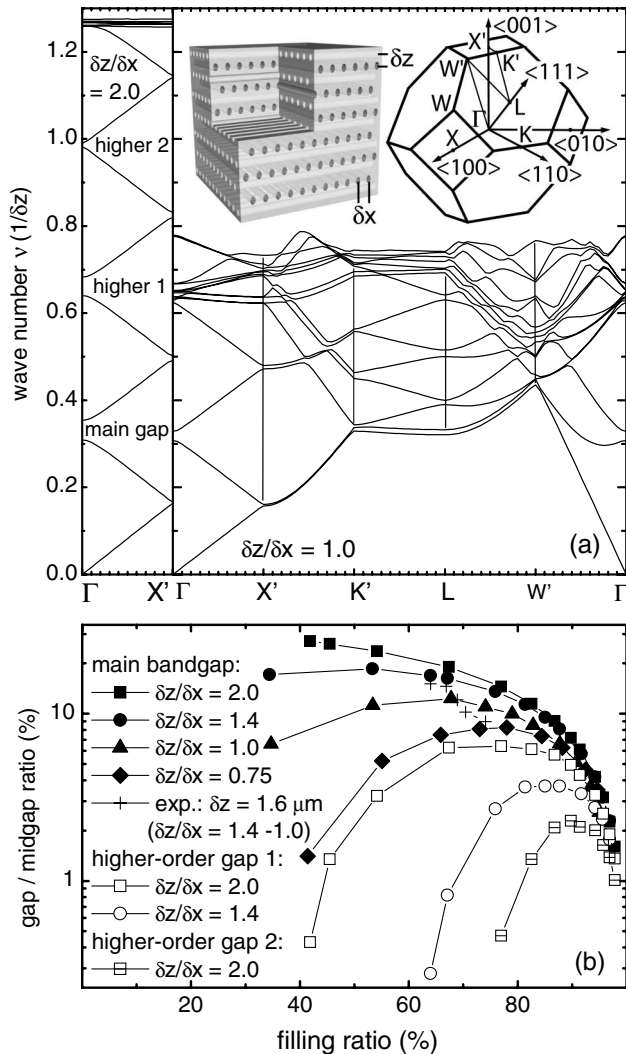

FIG. 1. (a) Photonic band structures of woodpile-type polymer void channel photonic crystals for ratios $\delta z/\delta x$ of 1.0 (right) and 2.0 (left, only $\Gamma X'$), as calculated for $\delta z = 2.5$ μm and elliptical channel cross section of diameters 750 nm and 1.125 μm. The number of higher-order gaps strongly depends on $\delta z/\delta x$. Inset: Geometrical arrangement of void channels and corresponding first Brillouin zone. (b) Dependence of the gap/midgap ratio on the filling ratio for various values of $\delta z/\delta x$.
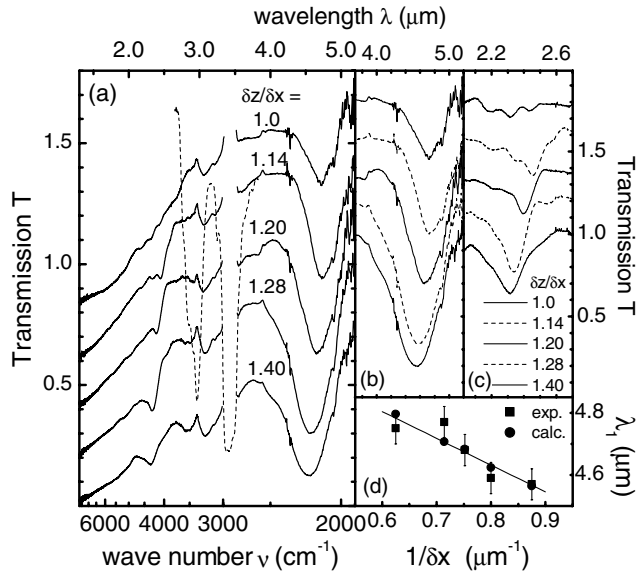
ing direction $\Gamma X'$). For consistency with experiments, diameters of 750 nm and 1.125 μm in the lateral and focusing directions and an effective refractive index of the solid resin of 1.65 were used. The insets in Fig. 1(a) show a sketch of the channel arrangement and the first Brillouin zone of the corresponding face-centred tetragonal (fct) lattice, which, however, is almost a cuboid for our ratios of $\delta z/\delta x$. Figure 1(b) presents the dependence of the gap/midgap ratio on the filling ratio (i.e., the polymer volume fraction of the crystals) for the fundamental and higher-order stop gaps as calculated for $\delta z/\delta x$ ranging from 0.75 to 2.0.

For symmetry reasons transverse electrical and magnetic modes have the same frequencies, and all photonic bands are degenerate. The wavelengths of the main gap and the higher-order gaps fulfill the Bragg condition:

$$m\lambda_{\mathrm{gap}} = 2\delta z n_{\mathrm{avg}} = 2\delta z[n - A/(\delta z \delta x)(n - 1)], \quad (1)$$

where m is the order of the gap, A the channel cross section, n_{avg} the average refractive index of the crystal, and n the effective refractive index of the polymer material after fabrication. The right side of Eq. (1) links the average refractive index to the woodpile structure geometry. The gap wavelengths vary linearly with the layer spacing and depend only indirectly on the in-plane channel spacing via the average refractive index. The order number m represents only even multiples of the smallest reciprocal vector in the stacking direction, because the geometrical structure factor vanishes otherwise due to destructive interference of contributions from perpendicular channels. However, a few forbidden modes in the $\Gamma X'$ direction result in minor gaps of order $m - 1/2$ [Fig. 1(a), left].

The calculations reveal a strong dependence of the number of higher-order gaps on $\delta z/\delta x$. For small $\delta z/\delta x$ only a main gap exists in the stacking direction. In some other directions stop gaps are also observed, but a complete band gap does not exist. With increasing $\delta z/\delta x$ gap/midgap ratios increase and higher-order gaps appear in the stacking direction, as higher photonic bands are shifted to larger wave numbers. While for $\delta z/\delta x = 1.0$ the first higher-order gap is just about to appear [Fig. 1(a), right], for $\delta z/\delta x = 1.4$ one single higher-order gap exists, and for $\delta z/\delta x = 2.0$ two such gaps are fully developed [Fig. 1(a), left, and Fig. 1(b)].

Experimentally, at first the main gap and the appearance of the first higher-order gap were investigated. Because the polymer material absorbs strongly beyond $\lambda = 5.5$ μm, a layer spacing of 1.6 μm was chosen with in-plane channel spacings varying from 1.14 to 1.6 μm ($\delta z/\delta x = 1.4$–1.0). These parameters result in main photonic stop gaps near 4.6 μm and higher-order gaps near 2.3 μm. Figure 2 presents the infrared transmission spectra [2(a)] as well as plots of the main gap [2(b)] and the first higher-order gap [2(c)] after the baseline

FIG. 2. Infrared spectra of woodpile structures at constant $\delta z = 1.6$ μm with δx varying from 1.14 to 1.6 μm. (a) As measured; dashed line: polymer absorption. (b) Fundamental photonic band gap and (c) first higher-order gap after baseline correction. (d) Linear dependence of the gap wavelength on the inverse in-plane channel spacing.

correction for scattering effects. Although the curves are a ratio of the spectra of the photonic crystal and a layer of the homogeneous polymer material of equal thickness, strong polymer absorption bands between 2.7 and 3.8 μm (dashed curve) still result in some minor artifacts. The main gaps suppress infrared transmission by up to 85%. Their gap/midgap ratios of up to 14% [Fig. 1(b), crossed symbols] are in good agreement with theory. Higher-order gaps have a depth of up to 40%. Their gap/midgap ratios of up to 7% exceed the theoretical values due to imperfections related to halos of compressed material and high NA focusing conditions. With decreasing $\delta z/\delta x$ main gap and higher-order gaps shift slightly to longer wavelengths, because the channel cross section was kept constant and, hence, the average refractive index of the structure increased. Figure 2(d) shows a plot of the main gap wavelength λ_1 vs $1/\delta x$, which according to Eq. (1) yields a linear dependence with $n = 1.663$ and $A = 0.62$ μm^2. Assuming an ellipsoidal cross section with a ratio of the semiaxes of 1.5, a lateral channel diameter of 744 nm can be derived. Band structure calculations reproduce the curve for a lateral diameter of 750 nm, a diameter of 1.125 μm in the focussing direction, and an effective refractive index $n = 1.678$. We attribute the higher effective refractive index of the material as compared to $n = 1.56$ for the cured polymer to the generation of compressed regions extending a few hundred nanometers into the channel vicinity [16]. From the Clausius-Mossotti relation $(n^2 - 1)/(n^2 + 2) = \alpha/3\upsilon\varepsilon_0$ an even stronger rise in the refractive index n is expected indicating a reduced polarizability α upon

compression of the material volume υ. As expected from Fig. 1, a decrease of $\delta z/\delta x$ gradually reduces the depth of the higher-order gap, until for $\delta z/\delta x = 1.0$ it has nearly disappeared.

In order to examine stop gaps of the order $m \geq 3$, we prepared samples at a fixed fct unit cell geometry (constant $\delta z/\delta x = 2.0$) with layer spacings varying from 2.4 to 2.7 μm. Figure 3 presents their transmission and reflection infrared spectra. The main gaps (not shown) are located around 7.8 μm. The first two higher-order gaps near 3.8 and 2.6 μm are easily recognized with a maximum suppression of infrared transmission of as much as 75% and 65%, respectively. In agreement with Fig. 1 a third higher-order gap at 2.0 μm is on the verge of appearance as seen by a 30% dip. The corresponding reflection spectra show large spikes in the stop gap regions, whereas almost no light is reflected elsewhere due to the low refractive index change at the crystal boundary. Consistent with Eq. (1), a 12.5% increase of the layer spacing from 2.4 to 2.7 μm results in a 15% increase of the higher-order gap wavelengths. A linear regression of $\lambda_{\text{gap}}/\delta z$ vs $1/\delta z^2$ yields $n = 1.631$ and 1.647 and lateral channel diameters of 716 and 748 nm using the first and second higher-order gaps, respectively [Figs. 3(c) and 3(d)]. The lower effective refractive index as compared
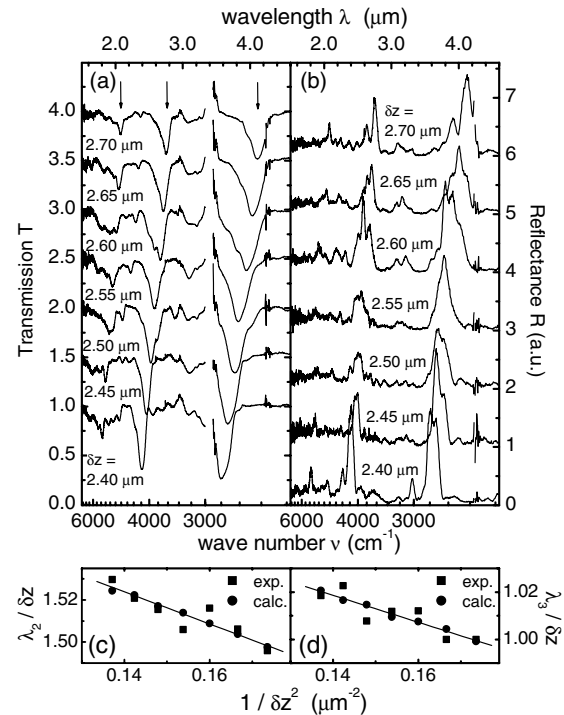

FIG. 3. Higher-order bandgaps in transmission (a) and reflection (b) for constant $\delta z/\delta x = 2.0$ with layer spacing δz varying from 2.4 to 2.7 μm. Dips in transmission correspond to spikes in reflection. (c) First and (d) second higher-order gap wavelengths as a function of δz with linear curve fit and photonic band theory results.
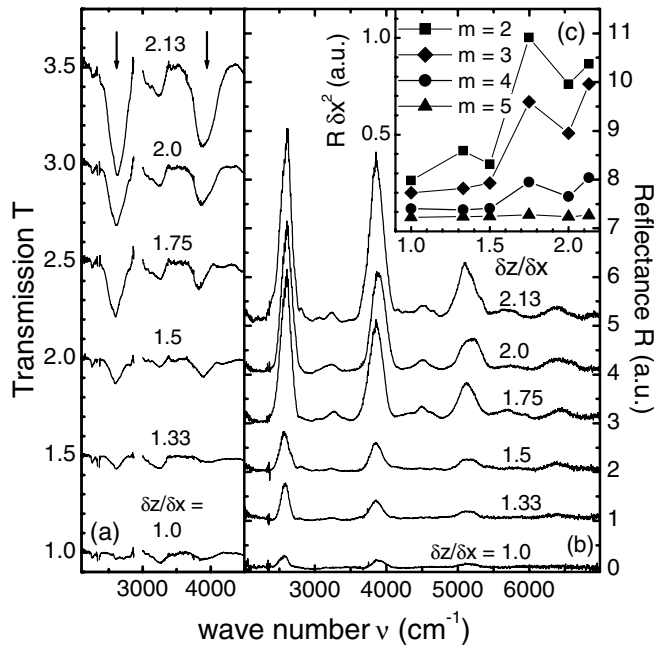
FIG. 4. (a) Transmission and (b) reflection infrared spectra at constant $\delta z = 2.55$ μm and varying unit cell geometry ($\delta z/\delta x = 2.13$–1.0). Note the emergence of higher-order band gaps ($m = 2, 3$) with increasing $\delta z/\delta x$. (c) Calibrated peak reflectances reveal the transformation of Bragg resonances into photonic band gap reflections.

to the series of samples at $\delta z = 1.6$ μm may be explained by the smaller fraction of compressed polymer material due to the larger lattice parameters.

The dependence of the higher-order stop gaps on the unit cell geometry is investigated in more detail in Fig. 4, which shows spectra for a series of crystals at constant $\delta z = 2.55$ μm with $\delta z/\delta x$ varying from 2.13 down to 1.0. As higher-order gaps correspond to higher harmonics of Bragg resonances, they are equally spaced on the wave number scale. The first two higher-order gaps in the transmission spectrum gradually disappear with decreasing $\delta z/\delta x$, the second faster than the first one (effects at shorter wavelengths were very small or negligible). In reflection at least four sharp spikes can be observed at multiples of the fundamental wave number. As photonic stop gaps provide total reflection for ideal infinite size crystals, such peaks are much higher as compared to mere resonant angle Bragg backscattering that can also be identified by its dependence on the number of contributing unit cells. Calibration of the peak heights to $(\delta x)^2$ renders mere Bragg reflections independent of the ratio $\delta z/\delta x$, as seen in Fig. 4(c) for the peak at λ_5. By contrast, the appearance of a stop gap leads to a strong rise in the calibrated reflectance, which is seen for the first higher-order gap above $\delta z/\delta x = 1.0$ with an additional strong jump between 1.5 and 1.75. For the second higher-order gap a similar jump is observed there, and even the peak at λ_4 is influenced by forbidden modes of light propagation

beyond $\delta z/\delta x = 1.5$. Again these findings are fully consistent with theory (Fig. 1). Moreover, note the small satellite peaks between the gap-related reflection spikes in Fig. 4(b), which correspond to the additional minor gaps in the middle between stop gaps of integer order m, as seen in Fig. 1(a) (left).

In conclusion, our experiments demonstrate that photonic crystals with a large number of higher-order stop gaps in the mid- and near-infrared spectral regions can be generated based on void channel microstructures with submicron channel diameters. In excellent agreement with band structure calculations, the number and size of the stop gaps observed are determined by the woodpile structure unit cell parameters. The efficient generation of such high quality polymer photonic crystals by femtosecond laser microfabrication bears a high potential for applications at telecommunication wavelengths, as optical properties of devices can be achieved at larger structural dimensions.

[1] A. Chelnokov, S. Rowson, J.-M. Lourtioz, L. Duvillaret, and J.-L. Courtaz, Electron. Lett. **33**, 1981 (1997).
[2] W. L. Vos and H. M. van Driel, Phys. Lett. A **272**, 101 (2000).
[3] P. V. Braun and P. Wiltzius, Nature (London) **402**, 603 (1999).
[4] A. Blanco, E. Chomski, S. Grabtchak, M. Ibisate, S. John, S. W. Leonard, C. Lopez, F. Meseguer, H. Miguez, J. P. Mondia, G. A. Ozin, O. Toader, and H. M. van Driel, Nature (London) **405**, 437 (2000).
[5] Y. A. Vlasov, X.-Z. Bo, J. C. Sturm, and D. J. Norris, Nature (London) **414**, 289 (2001).
[6] S. Rowson, A. Chelnokov, C. Cuisin, and J.-M. Lourtioz, IEE Proc. Optoelectron. **145**, 403 (1998).
[7] M. Straub and M. Gu, Opt. Lett. **27**, 1824 (2002).
[8] L. M. Goldenberg, J. Wagner, J. Stumpe, B.-R. Paulke, and E. Görnitz, Langmuir **18**, 3319 (2002).
[9] J. Wijnhoven, L. Bechger, and W. L. Vos, Chem. Mater. **13**, 4486 (2001).
[10] M. Egen and R. Zentel, Chem. Mater. **14**, 2176 (2002).
[11] Y.-H. Ye, F. LeBlanc, A. Hache, and V.-V. Truong, Appl. Phys. Lett. **78**, 52 (2001).
[12] J. Joannopoulos, R. Meade, and J. Winn, *Photonic Crystals* (Princeton University Press, New York, 1995).
[13] *Photonic Band Gap Materials*, edited by C. M. Soukoulis, NATO ASI, Ser. E, Vol. 315 (Kluwer Academic Publishers, Dordrecht, 1996).
[14] H. S. Sozuer, J. W. Haus, and R. Iguva, Phys. Rev. B **45**, 13 962 (1992).
[15] L. Liu, P. Li, and S. A. Asher, J. Am. Chem. Soc. **119**, 2729 (1997).
[16] M. J. Ventura, M. Straub, and M. Gu, Appl. Phys. Lett. **82**, 1649 (2003).
[17] S. G. Johnson and J. D. Joannopoulos, Opt. Express **8**, 173 (2001).